

# Preparation of Supercapacitor Electrodes through Selection of Graphene Surface Functionalities

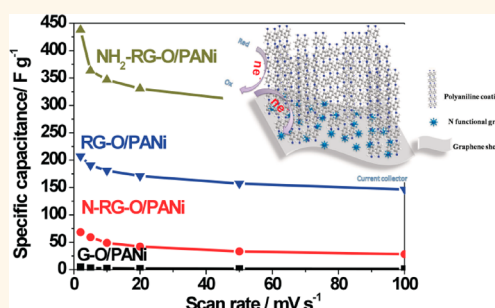
Linfei Lai,<sup>†,‡,§</sup> Huanping Yang,<sup>†</sup> Liang Wang,<sup>†</sup> Boon Kin Teh,<sup>†</sup> Jianqiang Zhong,<sup>⊥</sup> Harry Chou,<sup>§</sup> Luwei Chen,<sup>‡</sup> Wei Chen,<sup>⊥</sup> Zexiang Shen,<sup>†,\*</sup> Rodney S. Ruoff,<sup>§</sup> and Jianyi Lin<sup>†,‡,\*</sup>

<sup>†</sup>Division of Physics and Applied Physics, School of Physical and Mathematical Sciences, Nanyang Technological University, Singapore, 637371, Singapore, <sup>‡</sup>Institute of Chemical and Engineering Sciences, A\*STAR, 1 Pesek Road, Jurong Island, Singapore 627833, Singapore, <sup>§</sup>Department of Mechanical Engineering and Materials Science and Engineering Program, University of Texas at Austin, One University Station C2200, Austin, Texas 78712, United States, and <sup>⊥</sup>Department of Physics, Faculty of Science, National University of Singapore, 2 Science Drive 3, Singapore 117542, Singapore

Electrochemical supercapacitors have drawn much attention in recent years due to their high power density, reversibility, long cycle life, and small environmental impact.<sup>1</sup> They can be divided into two basic types according to their charge storage mechanism. The electric double-layer capacitance (EDLC) type generates capacitance from charge separation at the electrode/electrolyte interface,<sup>1,2</sup> while the pseudocapacitance type generates capacitance from fast Faradic reactions in the electrode material.<sup>3</sup> Porous carbonaceous materials are regarded as EDLC supercapacitors, where surface area, pore structure, and conductivity of the electrode are critical and Faradic reactions are not involved. Porous carbon supercapacitors feature long cycle life and good mechanical properties; they require materials with high surface area and pores adapted to ion size.<sup>1</sup> Metal oxides (e.g., RuO<sub>2</sub>,<sup>3</sup> MnO<sub>2</sub>,<sup>4</sup> and IrO<sub>2</sub>) and conducting polymers (e.g., polyaniline,<sup>5</sup> polypyrrole,<sup>6</sup> and polythiophene) are typical pseudocapacitive materials that can achieve relatively high capacitance but are limited by poor cyclability due to structural degradation of the electrode through the redox process.<sup>7,8</sup> Therefore, composites incorporating a porous carbon backbone coated with pseudocapacitive materials suggest a potential breakthrough for a new generation of supercapacitors.<sup>1</sup> Therefore research on carbonaceous materials loaded with metal oxides or polymers is widely reported.<sup>3,5,9,10</sup>

Polyaniline (PANI) is a highly promising electrode material due to its low cost, easy synthesis, good conductivity, fast redox rate, and high pseudocapacitance. It has been reported that when paired with

## ABSTRACT



In order to investigate the effect of graphene surface chemistry on the electrochemical performance of graphene/polyaniline composites as supercapacitor electrodes, graphene oxide (G-O), chemically reduced G-O (RG-O), nitrogen-doped RG-O (N-RG-O), and amine-modified RG-O (NH<sub>2</sub>-RG-O) were selected as carriers and loaded with about 9 wt % of polyaniline (PANI). The surface chemistry of these materials was analyzed by FTIR, NEXAFS, and XPS, and the type of surface chemistry was found to be important for growth of PANi that influences the magnitude of increase of specific capacitance. The NH<sub>2</sub>-RG-O/PANI composite exhibited the largest increase in capacitance with a value as high as 500 F g<sup>-1</sup> and good cyclability with no loss of capacitance over 680 cycles, much better than that of RG-O/PANI, N-RG-O/PANI, and G-O/PANI when measured in a three-electrode system. A NH<sub>2</sub>-RG-O/PANI/N-RG-O supercapacitor cell has a capacitance of 79 F g<sup>-1</sup>, and the corresponding specific capacitance for NH<sub>2</sub>-RG-O/PANI is 395 F g<sup>-1</sup>. This research highlights the importance of introducing -NH<sub>2</sub> to RG-O to achieve highly stable cycling performance and high capacitance values.

**KEYWORDS:** supercapacitor electrodes · graphene · surface functionalities

various electrode materials such as carbon,<sup>11</sup> metal,<sup>12</sup> or metal oxides<sup>13</sup> in supercapacitors, PANi can greatly enhance the capacitance of the modified electrodes.<sup>11</sup> Additionally, the stability, conductivity, and redox behavior of PANi may be also improved by the presence of carbon. This enhancement depends on the morphology and pore structure of the modified electrode material, which can be measured in the specific surface area, electronic properties, and ion diffusivity.<sup>15</sup>

\* Address correspondence to zexiang@ntu.edu.sg; lin\_jianyi@ices.a-star.edu.sg.

Received for review February 23, 2012 and accepted May 25, 2012.

Published online May 26, 2012  
10.1021/nn3008096

© 2012 American Chemical Society

As a carbon nanomaterial, graphene exhibits many unusual and attractive physical, chemical, and mechanical properties. In particular, these properties make graphene a stronger candidate electrode material for supercapacitor applications than ordinary porous carbon, activated carbon, and carbon nanotubes.<sup>14</sup> Graphene/PANi composites have shown higher capacitances than activated-carbon/PANi and carbon-nanotube/PANi composites.<sup>15–17</sup>

Graphene/PANi composites can be produced by *in situ* chemical oxidative polymerization of aniline using graphene oxide (G-O) or reduced graphene oxide (RG-O) as carriers. Pure graphene is not easily dispersed in aqueous solutions, which limits its application, and to date, a scalable method of making pure graphene flakes has not been reported. To solve this problem, surface-modified graphenes with various functional groups are used to prepare graphene/PANi composites, among which G-O is the most easily synthesized and most widely employed. G-O contains a large amount of oxygen functional groups such as OH, CO, COC, and COOH.<sup>18</sup> These groups aid dispersion of G-O in solution and aniline monomer adsorption, which favors achieving a uniform coating of PANi on G-O. It was also reported that carboxyl groups from G-O could link to the nitrogen atoms in the PANi backbone, providing doping for the interaction in addition to bonding and, thus, taking the place of an additional dopant such as Cl<sup>-</sup>.<sup>19</sup> Nevertheless, the poor electrical conductivity of G-O will hinder efficient charge transfer in the graphene network and reduce cyclability.<sup>20</sup> This drawback can be overcome by chemical reduction or by thermal annealing to partly remove O-containing groups, thus partially restoring the graphene sp<sup>2</sup> network.<sup>21,22</sup> It is obvious that the graphene surface functionalities are important to the performance of supercapacitors. However, little work has been reported investigating the effect of graphene surface chemistry on PANi loading and the effect of such loading on capacitive performance.

In this paper, four different surface-functionalized graphenes, graphene oxide (G-O); reduced G-O (RG-O); nitrogen doped graphene (N-RG-O), and primary amine-modified graphene (NH<sub>2</sub>-RG-O), were synthesized for use in “graphene”/PANi composites. In an attempt to achieve the highest synergistic effect between the chemically modified graphenes and PANi, the amount of conducting polymer loading was fixed at ~10 wt %. This value was chosen to prevent the blockage of micropores and the degradation of the graphene composite conductivity from excessive polymer loading. Among the four samples, NH<sub>2</sub>-RG-O showed an 8-fold capacitance increase after PANi loading. The 500 F g<sup>-1</sup> capacitance of NH<sub>2</sub>-RG-O/PANi was larger than that of G-O/PANi (4.7 F g<sup>-1</sup>), N-RG-O/PANi (68.47 F g<sup>-1</sup>), and RG-O/PANi (207.11 F g<sup>-1</sup>). Moreover, the NH<sub>2</sub>-RG-O/PANi composite exhibited

an unusually good cyclability and an increase in capacitance by a factor of 1.19 after 680 cycles at 2 mV s<sup>-1</sup>. The effect of –NH<sub>2</sub> functional groups on the preparation and electrochemical performance of “graphene”/PANi supercapacitors was carefully studied and elucidated for this paper.

## RESULTS AND DISCUSSION

The surface character of the different chemically modified graphenes was identified by Fourier transform infrared spectra (FT-IR), X-ray absorption spectroscopy (XAS), and X-ray photoelectron spectroscopy (XPS). G-O contains a wide range of oxygen functional groups both on the basal planes and at the edges of the G-O sheets.<sup>23</sup> The FT-IR spectrum (Figure S1a) of G-O demonstrates the presence of C–O in carbonyl ( $\nu_{\text{C-O}}$  at 1056 cm<sup>-1</sup>), C–O in carboxylic acid ( $\nu_{\text{C-O}}$  at 1162 cm<sup>-1</sup>), and C–O–C ( $\nu_{\text{C-O}}$  at 1226 cm<sup>-1</sup>), C–OH ( $\nu_{\text{C-O}}$  at 1307 cm<sup>-1</sup>), and C=O in carboxylic acid and carbonyl moieties ( $\nu_{\text{C=O}}$  at 1631 and 1730 cm<sup>-1</sup>), in addition to the strong C=C stretching deformation of a honeycomb carbon network at 1497 cm<sup>-1</sup>. After the G-O is reduced by NaBH<sub>4</sub>, the peak intensities of C–O (1056 cm<sup>-1</sup>) and C=O (1631 and 1730 cm<sup>-1</sup>) decrease significantly while the C=C graphene network vibration remains strong around 1600 cm<sup>-1</sup>. A broad band of strong absorption around 1200 cm<sup>-1</sup> is due to the overlap of B–C vibration (1225 cm<sup>-1</sup>) and –OH vibration (1200 cm<sup>-1</sup>); this indicates the introduction of boron from the NaBH<sub>4</sub> reduction reaction and an incomplete reduction of G-O. NH<sub>2</sub>-RG-O was prepared *via* a solvothermal process in which ammonia–water reacted with G-O in the presence of ethylene glycol. Ammonium ions in ammonia–water can attack the oxygenated groups of G-O and generate primary amine groups at the NH<sub>2</sub>-RG-O surface by nucleophilic replacement.<sup>21</sup> The ethylene glycol in the solvothermal system functions as a reducing agent and assists the removal of oxygenated groups in the G-O. For NH<sub>2</sub>-RG-O samples (Figure S1b), the two distinct vibration bands besides the characteristic C=C peaks are IR absorptions at 1565 and 2800–2980 cm<sup>-1</sup>; the former is the sp<sup>2</sup> C=N bond, while the latter is the C–H stretching vibration of the NH<sub>2</sub>–G bond. N-RG-O was produced from a reaction between G-O and NH<sub>3</sub> gas at high temperatures, ~550 °C (*vs* <200 °C for NH<sub>2</sub>-RG-O). During this synthesis process some C–C and C–O bonds may rupture, forming pyridinic and graphitic C–N species in the N-RG-O. Hence, the nitrogen atoms in the N-RG-O sample exist mostly in the pyridinic and graphitic form, while in NH<sub>2</sub>-RG-O primary amine functional groups coexist with pyridinic nitrogen. NaBH<sub>4</sub> efficiently reduces G-O and can decrease the presence of oxygenated groups.<sup>22</sup> The C=N bond at 1565 cm<sup>-1</sup> is not observed in the IR spectrum of N-RG-O (Figure S1b) and indicates that NH<sub>2</sub>-RG-O has higher nitrogen

content than N-RG-O. From Figure S1 we can also conclude that RG-O, NH<sub>2</sub>-RG-O, and N-RG-O have very low oxygen content compared to G-O.

The carbon K-near-edge X-ray absorption fine-structure spectra of the four different surface-modified graphenes are shown in Figure 1. The graphite spectrum is displayed as a reference. The main peak around 285 eV can be assigned to the C K-edge  $\pi^*$  resonance and is observable in all five spectra. The strong peak at

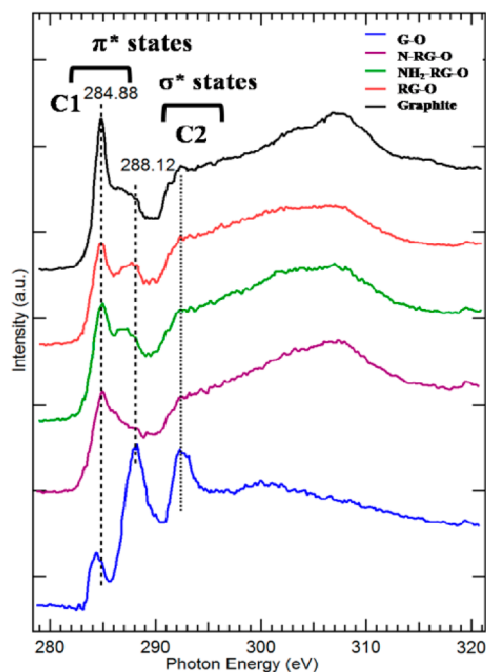


Figure 1. NEXAFS spectra at the C K-edge of G-O, RG-O, NH<sub>2</sub>-RG-O, and N-RG-O. The spectrum of graphite is also included for comparison.

293 eV is associated with the  $\sigma^*$  resonance, while higher energy absorption bands at 295–315 eV are due to the transitions from C1s to higher conduction  $\pi$  or  $\sigma$  states. The absorption peak between 286 and 290 eV may be attributed to an interlayer transition according to Pacile *et al.*<sup>24</sup> and/or the presence of COOH and alkyl functional groups as proposed by Jeong *et al.*<sup>25</sup> This peak is remarkably strong in the G-O spectrum, indicating a high concentration of COOH and CO species. The  $\sigma^*$  resonance feature at 293 eV is prominent in the G-O spectrum. This may be associated with the presence of a large amount of COC and COH groups, which are upright with respect to the carbon basal plane and therefore possess  $\sigma$  symmetry. It is noted that, compared to the other four samples, the main resonance of G-O at 284.8 eV is shifted to lower photon energy and a lower intensity, and both are indicative of more defects in the G-O sp<sup>2</sup> carbon network.<sup>26</sup> For RG-O, the intensity ratio between the peaks at 288.1 and 293 eV and the main resonance peak at 284.9 eV suggests the removal of oxygen-containing groups and the repair of the graphene  $\pi$  network. The C K NEXAFS spectra of NH<sub>2</sub>-RG-O and N-RG-O are basically similar to that of RG-O in that the attachment of NH<sub>2</sub> groups or incorporation of substitutional N to the carbon sp<sup>2</sup> network does not affect the C K-edge absorption directly.

Nitrogen K-near-edge X-ray absorption fine spectra of NH<sub>2</sub>-RG-O and N-RG-O are displayed in Figure 2a. Strong  $\pi^*$  resonance features at 397–403 eV and a strong broad  $\sigma^*$  resonance band between 403 and 425 eV are observed in both N-RG-O and NH<sub>2</sub>-RG-O. Three well-resolved peaks, denoted N1 (398.5), N2 (399.8), and N3 (401.5), are observable and agree with

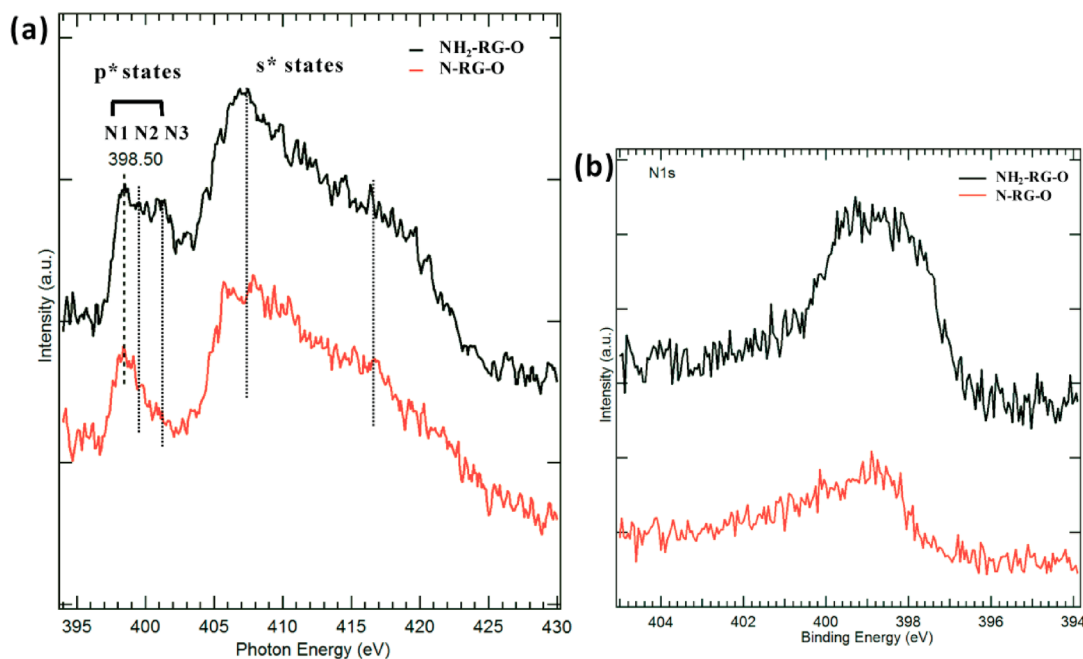


Figure 2. N K-edge NEXAFS spectra of NH<sub>2</sub>-RG-O and N-RG-O (a) and XPS of N 1s spectra of NH<sub>2</sub>-RG-O and N-RG-O (b).

peaks seen in similar studies in N-doped carbon and CN composites.<sup>27</sup> The N1 (398.5 eV) peak is attributed to pyridinic N atoms, which replace carbon atoms in the graphene layer but bond to only two carbon atoms and donate one electron to the carbon network (C=N=C  $\pi^*$ ). The N2 peak is assigned to primary amine-type nitrogen bonds (C-NH<sub>2</sub>).<sup>28–30</sup> N3 can be assigned to the  $\pi^*$  transition from N1s to admide N (–OCNH<sub>2</sub> or secondary admide–OCNHCO–) according to the *ab initio* calculation.<sup>20</sup> N2 and N3 are strong in NH<sub>2</sub>-RG-O but absent or weak in the N-RG-O spectrum. The strong peak located around 407 eV is assigned to the transition from the N1s core level to C–N  $\sigma^*$  states.<sup>27</sup> These N K-edge NEXAFS assignments are confirmed in the XPS N1s data. As shown in Figure 2b, the N 1s signal of N-RG-O is relatively weak at 398.5 eV and can be attributed to pyridinic nitrogen. For NH<sub>2</sub>-RG-O, in addition to the prominent pyridinic nitrogen peak at 398.3 eV, there exists a strong peak of primary amine functional groups at 399.5 eV and a minor component peak at 401.0 eV due to graphitic and/or amide N atoms.<sup>21</sup>

On the basis of the detailed analysis of XPS spectra, the surface elemental composition of these four graphene samples can be identified and quantified.

**TABLE 1. Portion of Chemical Species for Different Surface-Modified Graphene Based on XPS Results**

	G-O	RG-O	NH <sub>2</sub> -RG-O	N-RG-O
N			9.6	5.2
C	62.7	84.9	82.5	89.0
O	37.3	15.1	7.9	5.8

As summarized in Table 1, the G-O sample has an oxygen content of 37%, which is higher than RG-O (~15%), N-RG-O (~6%), and NH<sub>2</sub>-RG-O (~8%). The N-RG-O and NH<sub>2</sub>-RG-O samples have ~5% and 9% nitrogen, respectively (hydrogen is not taken into account for the calculation).

The electrochemical performance of the four graphene samples without PANi loading, *i.e.*, G-O, N-RG-O, NH<sub>2</sub>-RG-O, and RG-O, was evaluated by cyclic voltammetry in 1 M H<sub>2</sub>SO<sub>4</sub> electrolyte. The cyclic voltammetry (CV) curves of N-RG-O and NH<sub>2</sub>-RG-O as shown in Figure 3 have a nearly rectangular shape, which would be characteristic of a perfect EDLC. On the other hand, both RG-O and G-O exhibit a pair of redox peaks due to the transition between quinone/hydroquinone groups,<sup>1</sup> which is typical for carbon materials abundant in hydroxyl groups. The NH<sub>2</sub>-RG-O curve shows a current density of 2.5 A g<sup>-1</sup> at a scanning rate of 100 mV/s, which is larger than G-O (0.078 A g<sup>-1</sup>), N-RG-O (1.23 A g<sup>-1</sup>), and RG-O (2.0 A g<sup>-1</sup>). It is also noted that at high scan rates the increment of cathodic current to potential is sluggish Figure 3a; this demonstrates the poor conductivity of GO.

Figure 4 displays CV curves at various scan rates for the four graphene/PANi samples after loading ~9 wt % PANi. All of the graphene/PANi samples show a great increase in the current density compared to their counterpart graphenes without PANi. The capacitance can be calculated from the CV curves according to eq 1:

$$C = \frac{\left( \int idV \right)}{vmV} \quad (1)$$

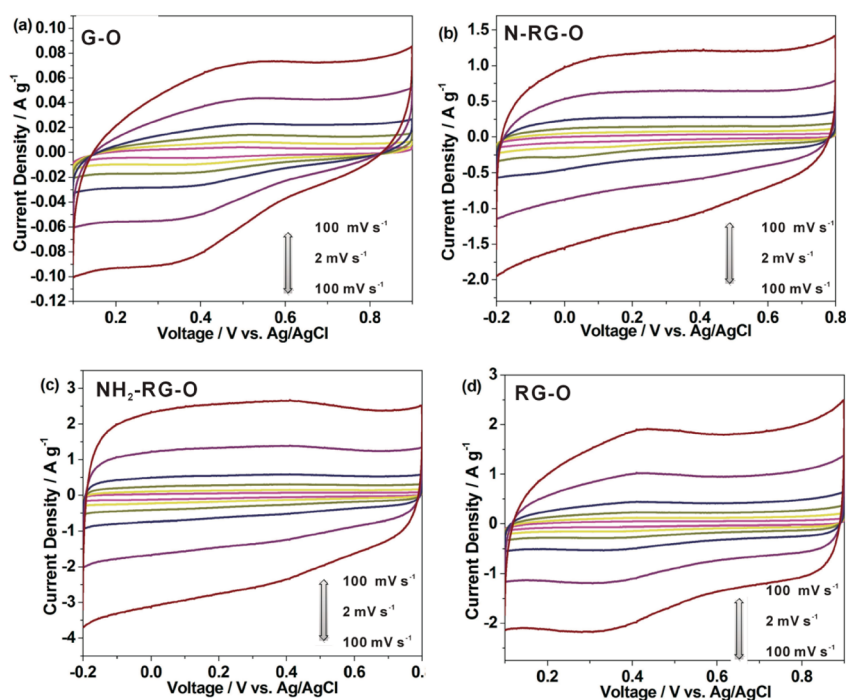


**Figure 3.** Cyclic voltammograms of G-O (a), N-RG-O (b), NH<sub>2</sub>-RG-O (c), and RG-O (d) recorded at different scan rates from 2 to 100 mV s<sup>-1</sup>.

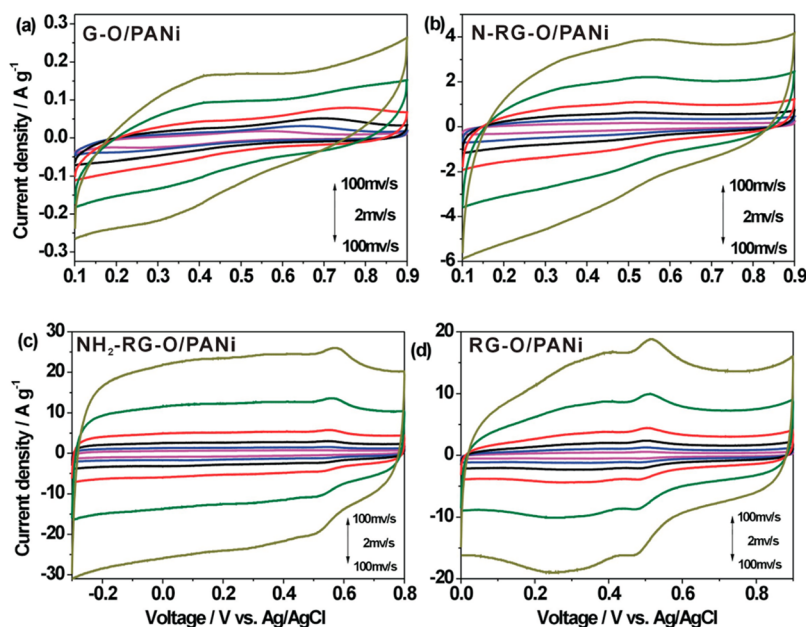


Figure 4. Cyclic voltammograms of G-O/PANI (a), N-RG-O/PANI (b), NH<sub>2</sub>-RG-O/PANI (c), and RG-O/PANI (d) recorded at different scan rates from 2 to 100 mV s<sup>-1</sup>.

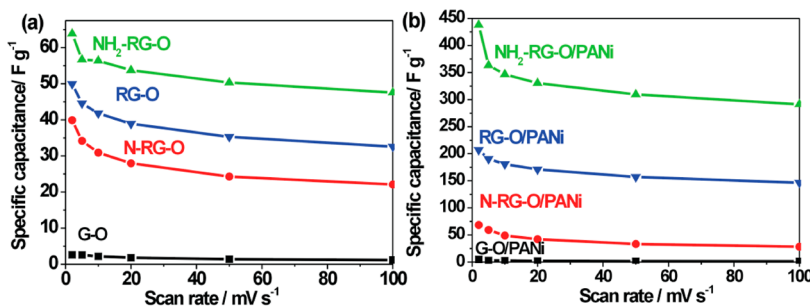


Figure 5. Specific capacitance of different surface-functionalized graphene before (a) and after (b) loading of 10 wt % PANi as a function of scan rate (from 2 to 100 mV s<sup>-1</sup>) in 1 M H<sub>2</sub>SO<sub>4</sub> electrolyte.

where  $i$  is the current density (A),  $V$  potential (V),  $v$  scan rate (mV s<sup>-1</sup>), and  $m$  mass of the graphene/PANI composite in the electrode (g).

As shown in Figure 5, NH<sub>2</sub>-RG-O increases its capacitance 8-fold due to the PANi loading, reaching 420 F g<sup>-1</sup> at a scan rate of 2 mV s<sup>-1</sup>. This is larger than that of G-O/PANI (4.7 F g<sup>-1</sup>), N-RG-O/PANI (68.47 F g<sup>-1</sup>), and RG-O/PANI (207.11 F g<sup>-1</sup>) under identical measurement conditions. BET surface areas of G-O/PANI, RG-O/PANI, NH<sub>2</sub>-RG-O/PANI, N-RG-O/PANI, and G-O are around 289, 265, 320, 358, and 310 m<sup>2</sup> g<sup>-1</sup>, respectively. The PANi/N-RG-O has the largest BET surface area and also relatively higher conductivity. However, the four samples do not show significant differences in BET value. Therefore, their different electrochemical behavior would come from the synergistic effect from both graphene and PANi. Note that the specific capacitance of NH<sub>2</sub>-RG-O/PANI is more than twice that of RG-O/PANI. The capacitance value of NH<sub>2</sub>-RG-O/PANI remains as high as 291 F g<sup>-1</sup> even under high scan rates of 100 mV s<sup>-1</sup>, which may be a

benefit of the high conductivity of the graphene/PANI composites.

Similar to those of pristine NH<sub>2</sub>-RG-O, the CV curves of NH<sub>2</sub>-RG-O/PANI are nearly rectangular in shape (Figure 4c) and indicate that both behave as electrochemical double-layer-type supercapacitors. A pair of new redox peaks (0.52/0.46 V with  $V = 0.057$  V) appear in NH<sub>2</sub>-RG-O/PANI, which represent the pseudocapacitance contribution of the PANi in the transformation from emeraldine to pernigraniline.<sup>17,31</sup> It is important to note that the cathodic and anodic peak positions of NH<sub>2</sub>-RG-O/PANI do not shift with the change in potential sweep rates, indicating fast pseudocapacitive charge transfer from PANi to NH<sub>2</sub>-RG-O. As the pseudocapacitive charge producer, PANi can generate capacitance values that are several times larger than those of reduced graphene oxide.<sup>18,32,33</sup> However, the polymer in the polymer/graphene composite normally leads to low percolation thresholds; in other words, only the top layers of the composite can contribute to the capacitance. Graphene serving as the current

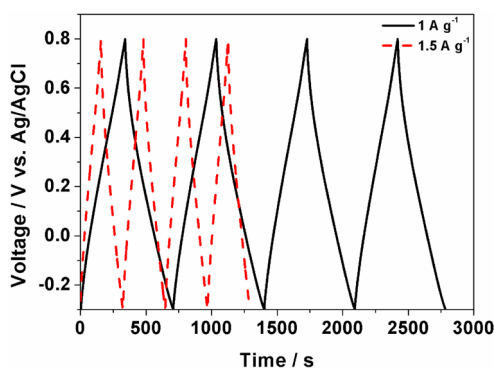


Figure 6. Galvanostatic charge/discharge curves of  $\text{NH}_2\text{-RG-O/PANi}$  at a current density of 1 and  $1.5 \text{ A g}^{-1}$  in  $1 \text{ M H}_2\text{SO}_4$  with a potential range from  $-0.3$  to  $0.8 \text{ V}$ .

collector provides active sites for electrical current to pass between layers. Recent reports showed that composite electrodes with thin film ( $<10 \text{ nm}$ ) conducting polymers were effective for fully reversible and rapid Faradic reactions; thus the conducting polymers contribute as pseudocapacitive charge storage.<sup>34,35</sup> On the contrary, Gomez *et al.* have recently reported that the redox peaks in the CV curves shift position with scan rate changes.<sup>15</sup> This may be due to high PANi loading (PANi to graphene ratios of 50–100%) and poor charge transfer between the PANi and graphene carrier.<sup>9</sup> In our experiments, the weight ratio of PANi was kept at a moderate level of  $\sim 9\%$  so that the prepared  $\text{NH}_2\text{-RG-O/PANi}$  electrode could act as highly conducting microelectrodes for electron transport from PANi to the chemically modified graphenes.  $\text{RG-O/PANi}$  (Figure 4d) also shows characteristic redox peaks at  $0.52$  and  $0.46 \text{ V}$ , which represent a Faradic reaction in the conducting polymer. Nevertheless, the CV curve shows nonidealities, particularly at high scan rates, indicating reduced conductivity of the RG carrier in comparison to  $\text{NH}_2\text{-RG-O/PANi}$ . The CV curves (Figures 4a and b) of  $\text{G-O/PANi}$  and  $\text{N-RG-O/PANi}$  are shallow with low current density ( $0.2\text{--}4$  vs  $15\text{--}20 \text{ A g}^{-1}$  for  $\text{NH}_2\text{-RG-O/PANi}$  and  $\text{RG-O/PANi}$ ) and deviate from a rectangular shape. Their measured capacitances are 8–10 times smaller than that of  $\text{NH}_2\text{-RG-O/PANi}$ .

Figure 6 shows the galvanostatic charge/discharge profiles of  $\text{NH}_2\text{-RG-O/PANi}$  at current densities of 1 and  $1.5 \text{ A g}^{-1}$ . The linear symmetric charging and discharging profiles indicate that the capacitive behavior of  $\text{NH}_2\text{-RG-O/PANi}$  is fully reversible. This composite also demonstrates fast charge transfer and redox kinetics. The specific capacitance is calculated using eq 2:

$$C = \frac{i\Delta t}{m\Delta V} \quad (2)$$

where  $i$  is the discharge current,  $\Delta t$  discharge time,  $m$  mass of the active material (weight of PANi + graphenes), and  $\Delta V$  the potential window, which is 388 and  $372 \text{ F g}^{-1}$  at 1 and  $1.5 \text{ A g}^{-1}$ , respectively,

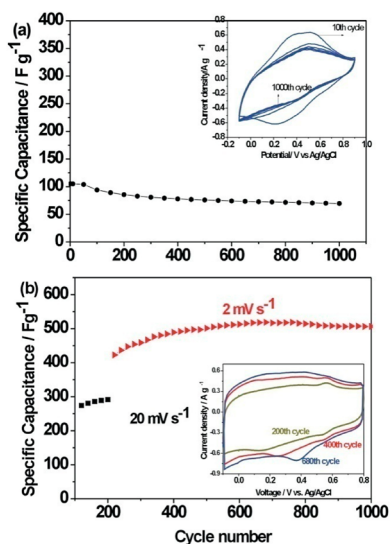


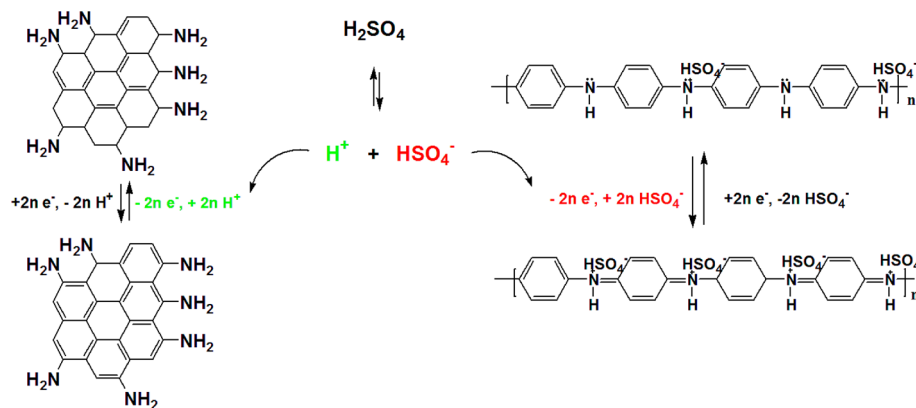
Figure 7. Cyclic-life data of  $\text{RG-O/PANi}$  electrode (a) and  $\text{NH}_2\text{-RG-O/PANi}$  (b). The specific capacitance value is calculated from CV curves at a scan rate of  $50 \text{ mV s}^{-1}$  in  $1 \text{ M H}_2\text{SO}_4$  electrolyte. Inset figure shows the CV curves during the 1000 cycles.

which agrees well with the values calculated from the CV curves using eq 1.

A stability study of  $\text{NH}_2\text{-RG-O/PANi}$  and  $\text{RG-O/PANi}$  was performed by cyclic voltammetry.  $\text{RG-O/PANi}$  exhibits a decay in the capacitance with increasing cycle number (see Figure 7a). An interesting phenomenon is observed with  $\text{NH}_2\text{-RG-O/PANi}$ , where the specific capacitance increases significantly with increasing cycle number (Figure 7b). After 100 cycles of charge/discharge activation at a scan rate of  $50 \text{ mV s}^{-1}$ , the CV curves were recorded at scan rate  $20 \text{ mV s}^{-1}$  from 120 to 220 cycles and then at scan rate of  $2 \text{ mV s}^{-1}$  from 220 to 680 cycles. The different scan rates were adapted in order to shorten the activation time period. Note that the capacitance value gradually increases from  $420 \text{ F/g}$  initially to  $500 \text{ F/g}$  at 200 cycles and remains stable up to 680 cycles.

High conductivity with reversible redox properties is regarded as necessary to achieve supercapacitors with long cycle-life. Increases in the capacitance with cycling number were reported previously with a  $\text{MWCNT-GO}$  composite. In that system, the improved conductivity was reasoned to be due to the reduction of oxygen content in GO with increasing cycles.<sup>36</sup> In our case, the capacitance increase is possibly due to the doping and dedoping of sulfate ions on the PANi polymer assisted by the simultaneous fast Faradic reactions of primary amine with  $\text{H}^+$ . The doping and dedoping of ions during the oxidation and reduction of PANi is responsible for the pseudocapacitive charge generation in these capacitors.

In previous reports, researchers found that the presence of heteroatoms, especially widely used N compounds, in the carbon network improved capacitance



Scheme 1. Faradic reactions of PANi and NH<sub>2</sub>-RG-O in acidic electrolyte.

and were the origin of stable pseudo-Faradaic reactions. In our recent studies, we find that the amine functional groups in NH<sub>2</sub>-RG-O react with protons to produce imine or protonated amine,<sup>21</sup> while the consumption of H<sup>+</sup> in electrolyte helps H<sub>2</sub>SO<sub>4</sub> → HSO<sub>4</sub><sup>-</sup> dissociation. The amine redox reactions can therefore assist charge doping and dedoping in PANi. This synergistic effect can result in the doubled charge storage processes as shown in Scheme 1.

Controlling the carbon surface chemistry is of significant importance when growing polymer on the carbon carrier. Fang *et al.* reported that the modification of carbon could improve its wettability and further enhance its electrochemical performance in supercapacitors.<sup>37</sup> While the chemical content and type of surface groups have a pronounced effect on the capacitance,<sup>38</sup> only basic or neutral groups such as phenol and ethers were thought to be able to improve capacitance.<sup>39</sup> NH<sub>2</sub>-RG-O and RG-O contain unreduced hydroxyl groups, which are advantageous for supercapacitors. N-RG-O, which was reduced under an inert gas atmosphere, was doped with graphitic and pyridinic nitrogen atoms with poor wettability. GO holds a high concentration of oxygen functionalities, but the poor conductivity severely hinders it for electrochemical applications. Therefore, NH<sub>2</sub>-RG-O and RG-O, containing N heteroatoms, can improve the capacitance of the electrode, with unreduced hydroxyl groups on NH<sub>2</sub>-RG-O also possibly contributing to the capacitance.

Electrochemical impedance spectroscopy (EIS) was used to measure the internal resistance, charge transfer kinetics, and ion diffusion process of the four graphene/PANi composites. The EIS was measured over a frequency range of 10 kHz to 10 mHz. As shown in the Figure 8 inset, the intercept between the impedance spectrum and real impedance axis (Z') is almost the same (0.035 Ohm) for all four graphene/PANi electrodes. This indicates that the series resistance, which includes the electrolyte solution resistance and contact resistance at the interface of active material/current collector, is very low for all four

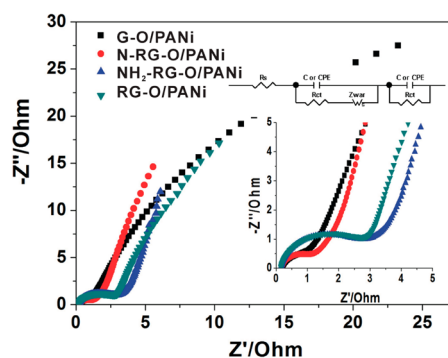


Figure 8. Electrochemical impedance plots of G-O/PANi, N-RG-O/PANi, NH<sub>2</sub>-RG-O/PANi, and RG-O/PANi. The spectra were taken in 1 M H<sub>2</sub>SO<sub>4</sub> in a frequency range from 10 kHz to 10 mHz. A Randles equivalent circuit representing the circuit elements for the Nyquist plot is shown in the inset. *R* is solution resistance, C or CPE represents double-layer capacitance or constant phase element, *R*<sub>ct</sub> is charge transfer resistance, and *Z*<sub>war</sub> is diffusion-controlled Warburg impedance.

graphene/PANi cells. The Nyquist plots in Figure 8 exhibit an incomplete semicircle in the high-frequency region and a vertical linear feature in the mid- to low-frequency region.

Among the four graphene/PANi composites, the vertical curve of NH<sub>2</sub>-RG-O/PANi has the largest slope with respect to the Z' axis, *i.e.*, closest to the imaginary impedance axis (Z''), which implies that NH<sub>2</sub>-RG-O/PANi exhibits the highest conductivity or lowest internal resistance, including polarization impedance. In contrast, the low-frequency Nyquist plot of G-O/PANi is almost 45 degrees with respect to Z'. That is, the real and imaginary components of the impedance vector are almost equal at all frequencies, which is a characteristic of Warburg impedance, where ion diffusion effects at the electrolyte/electrode interfaces dominate the electrochemical reaction mechanism on the G-O/PANi electrode. The structural defectivity and abundance of oxygen-containing groups in G-O that hinder the ion diffusion through the G-O/PANi layers are the main reasons for the high Warburg impedance. The Nyquist plots in the high-frequency region in Figure 8a

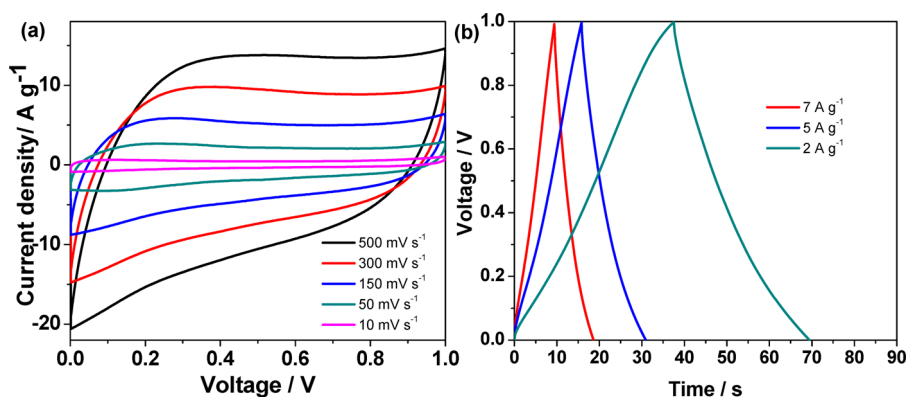


Figure 9. (a) Cyclic voltammograms taken at various scan rates of 10–500  $\text{mV s}^{-1}$  and (b) Galvanostatic charge/discharge curves taken between 0 and 1 V at various constant currents of 2–7  $\text{A g}^{-1}$  for the asymmetric capacitor  $\text{NH}_2\text{-RG-O/PANi//N-RG-O}$  in 1 M  $\text{H}_2\text{SO}_4$ .

resemble an incomplete semicircle. The semicircle impedance plots have been reported for many carbon, carbon nanotube, and graphene-based supercapacitors.<sup>40–42</sup> They can be well-modeled using a complex equivalent circuit, as shown in the inset in Figure 8.  $R_s$  is the series solution resistance, which may include the electrolyte resistance and the active material/current collector contact resistance. Two capacitors  $C$  (or more realistically, two constant phase elements, CPE, which take into consideration the electrode surface inhomogeneity) represent double-layer capacitance and Faradic capacitance, respectively.  $R_{ct}$ , in parallel to  $C$ , is the charge transfer resistance at the electrode/solution interface, while  $Z_{war}$  is the ion diffusion-controlled Warburg impedance.

These components form a mixed control Randles circuit, which is usually used to model capacitance in a process with a combination of kinetic and diffusion processes determining the rate. The second capacitance circuit consists of a capacitor impedance  $C$  and charge transfer resistance  $R_{ct}$ . At high frequencies, the capacitor impedance becomes much smaller and the system resistance is dominated by the resistors and polarization impedances. At low frequencies, an ideal polarizable capacitance would give a straight line with large angles with respect to  $Z'$  or almost parallel to  $Z''$ . It is noted that in Figure 8 the semicircles partially (in the midfrequency region) disappear. The absence of the semicircle in the complex impedance plane has been reported and is explained by high ionic conductivity at the electrode/electrolyte interface.<sup>43</sup>

In the  $\text{NH}_2\text{-RG-O/PANi}$  case, when the frequency decreases and the impedance vector moves further from ( $Z' = 3 \text{ ohm}$ ,  $Z'' = 1 \text{ ohm}$ ), the phase angle does not decrease as in an ideal semicircle. Rather, the phase angle increases continuously with further decreases in frequency. This means that the polarization impedance reduces its contribution (*i.e.*, the kinetic and charge transfer are no longer rate-determining steps), while mass capacitance remains the dominant component of the system impedance. Hence the EIS data are

consistent with the other electrochemical measurements shown and discussed above, and they indicate that  $\text{NH}_2\text{-RG-O/PANi}$  is the best electrode material for supercapacitor applications, demonstrating low internal resistance, very good charge transfer, and excellent ionic conductivity.

It is known that the three-electrode cell used for evaluating the electrochemical performance of an active material usually shows a high sensitivity to Faradic reactions. This may lead to large errors in estimating the energy storage capability of the electrode material for supercapacitor applications.<sup>44</sup> It should be mentioned that it is difficult to achieve a high specific capacitance value if the supercapacitor cells are fabricated using a single conducting-polymer-based active material for both the cathode and anode. Therefore, we used N-RG-O as the cathode material and  $\text{NH}_2\text{-RG-O/PANi}$  as the anode electrode. The electrochemical performance of the  $\text{NH}_2\text{-RG-O/PANi//N-RG-O}$  cell is measured in 1 M  $\text{H}_2\text{SO}_4$  (Figure 9). The capacitance of the full cell is 35, 43, 52, 69, and 79  $\text{F g}^{-1}$  during scan rates of 500, 300, 150, and 10  $\text{mV s}^{-1}$ .

The specific capacitance per mass of one pellet electrode is calculated according to eq 3:

$$C_{\text{spec}} = 2C/m \quad (3)$$

where  $C$  is the experimental measured capacitance of the supercapacitor and  $m$  is the mass percentage of the  $\text{NH}_2\text{-RG-O/PANi}$  electrode. Therefore, the specific capacitance of the  $\text{PANi-NH}_2\text{-RG-O}$  electrode under scan rates of 500, 300, 150, 50, and 10  $\text{mV s}^{-1}$  are 175, 213, 261, 346, and 395  $\text{F g}^{-1}$ , respectively, which were higher than those reported for  $\text{PANi/CNT}$  (320  $\text{F g}^{-1}$ ) in a two-electrode testing environment,<sup>45</sup> but in our case the loading weight ratio of PANi decreased to  $\sim 10\%$ . At a charge/discharge rate of 2.0, 5.0, and 7.0  $\text{A g}^{-1}$ , they are 69.4, 56, and 48  $\text{F g}^{-1}$ , while the specific capacitances of the  $\text{PANi-NH}_2\text{-RG-O}$  electrode are 345, 280, and 240  $\text{F g}^{-1}$  respectively.

The results agree well with the values calculated from the CVs. At a charge/discharge rate of 2.0  $\text{A g}^{-1}$ ,

the energy density of our two-electrode cell can be as high as  $9.6 \text{ Wh kg}^{-1}$ , as calculated from  $E = CV^2/2$ . The cycling performance, which is analyzed by galvanostatic charge/discharge of the  $\text{NH}_2\text{-RG-O/PANI}/\text{N-RG-O}$  cell under  $1.0 \text{ V}$  with a current density of  $2 \text{ A g}^{-1}$ , gave a 85% capacitance maintained after 1000 cycles.

## CONCLUSION

Four different surface-functionalized graphenes were used as carriers for preparing chemically modified graphene/PANI composites. The largest capacitance of  $500 \text{ F g}^{-1}$  (all values are with respect to the combined mass of PANi and chemically modified graphene, which are derived from measurements on a three-electrode cell) was measured for a " $\text{NH}_2\text{-RG-O/PANI}$ " composite, which was an 8-fold improvement over a " $\text{NH}_2\text{-RG-O}$ " without PANi loading composite

and was much larger than that of " $\text{G-O/PANI}$ " ( $4.7 \text{ F g}^{-1}$ ), " $\text{N-RG-O/PANI}$ " ( $68.47 \text{ F g}^{-1}$ ), and " $\text{RG-O/PANI}$ " ( $207.11 \text{ F g}^{-1}$ ). Most importantly, a factor of 1.19 increase in capacitance was observed for  $\text{NH}_2\text{-RG-O/PANI}$  as the cycle number increased to 680 cycles, while the capacitance decay with increasing cycle numbers was measured for the other three graphene/PANI composites. The amine functional groups in  $\text{NH}_2\text{-RG-O}$  react with protons to produce imine or protonated amine, while the consumption of  $\text{H}^+$  in the electrolyte helps  $\text{H}_2\text{SO}_4 \rightarrow \text{HSO}_4^-$  dissociation. The amine redox reactions can therefore assist the doping and dedoping in PANi and might be responsible for the increased capacitance in long cycling. Introducing  $-\text{NH}_2$  into the carbon honeycomb network before loading the PANi helps the PANi/graphene composite to achieve high capacitance values for supercapacitor applications.

## METHODS

**Synthesis of Graphene Oxide (G-O).** Graphite oxide was prepared from natural flake graphite powder per a technique that has been reported elsewhere.<sup>20</sup> Briefly, 5 g of graphite and 3.5 g of  $\text{NaNO}_3$  were placed in a flask. Then 350 mL of  $\text{H}_2\text{SO}_4$  was added with stirring in an ice-bath environment, and 10 g of  $\text{KMnO}_4$  was added with vigorous stirring for 2 h. The mixture was kept for 6 days at room temperature. A 200 mL amount of 5 wt %  $\text{H}_2\text{SO}_4$  was then added to the mixture, and the system was kept at  $98^\circ\text{C}$  under reflux for 2 h. When the temperature was reduced to  $50^\circ\text{C}$ , 10 mL of  $\text{H}_2\text{O}_2$  (30 wt % aqueous solution) was added to terminate the reaction. The resultant mixture was purified by repeating the following procedure: washing (1 L of 3 wt %  $\text{H}_2\text{SO}_4$ ), followed by  $\text{H}_2\text{O}$  under centrifugation until the supernatant is colorless with a pH value around 6.0. Then the product is dispersed to 5 mg/mL under ultrasonication (140 W for 2 h) and freeze-dried for further use.

**Synthesis of  $\text{NH}_2\text{-RG-O}$ .**  $\text{NH}_2\text{-RG-O}$  was prepared with a method developed by our group.<sup>21</sup> A 100 mg portion of G-O was added to 40 mL of ethylene glycol under ultrasonication. After further addition of 1 mL of ammonia–water, the dark brown solution was transferred to a Teflon-lined autoclave for solvothermal reaction at  $180^\circ\text{C}$  for 10 h. The precipitate from the reaction was then filtered, washed repeatedly with distilled water, and dried at  $60^\circ\text{C}$  for further use. Since the reactant G-O platelets are subjected to temperatures that are capable of reducing them, we label this product as " $\text{NH}_2\text{-RG-O}$ ".

**Synthesis of N-RG-O and RG-O.** N-RG-O was prepared by annealing G-O at  $550^\circ\text{C}$  under  $\text{NH}_3$  gas flow. Briefly, 500 mg of G-O was put in a tube furnace with 5%  $\text{NH}_3$  in Ar flow of 50 sccm. It was then heated to  $550^\circ\text{C}$  in 20 min and kept at this temperature for half an hour. The resultant samples were ground, washed repeatedly with distilled water, and dried at  $60^\circ\text{C}$  for 24 h for further use. RG-O was prepared by chemical reduction: 500 mg of G-O powder was dipped in aqueous  $\text{NaBH}_4$  (50 mM) solution for 2 h. The resultant sample was washed repeatedly with distilled water and dried at  $60^\circ\text{C}$ .

**Synthesis of Various PANi/Graphene Composites.** The PANi/graphene composites were synthesized *via in situ* oxidative polymerization of aniline on the four different surface-functionalized graphenes by using ammonium persulfate as an oxidant. The aniline monomer was doubly distilled before use. A 200 mg amount of each type of functionalized graphene was individually ultrasonically dissolved in 20 mL of methanol. Then 2.38 mL of 0.1 M aniline in methanol was added drop by drop

into the solution, which was contained in an ice bath under magnetic stirring. After another 10 min, 4.76 mL of 0.02 M ammonium persulfate and 0.2 M  $\text{LiClO}_4$  in 1 M  $\text{H}_2\text{SO}_4$  was dripped in. The solution was shielded from light and kept in an ice bath, with magnetic stirring for 8 h to achieve full polymerization. The product was repeatedly washed with water, ethanol, and acetone to remove the residual oxidant. All of the composites were dried at  $60^\circ\text{C}$ .

**Characterization.** The near-edge X-ray adsorption fine-structure (NEXAFS) measurements were carried out at the Surface, Interface, and Nanostructure Science beamline of the Singapore Synchrotron Light Source. A total-electron yield mode with photon energy resolution of 0.1 eV was used. The XPS was collected with a Kratos Axis Ultra DLD (delay line detector) spectrometer. This XPS has a monochromatic Al K $\alpha$  X-ray source with a resolution of 0.1 eV. Fourier transform infrared spectra (FT-IR) were recorded on a Shimadzu IR Prestige-21 FTIR spectrophotometer.

The electrochemical performance of the samples was measured by cyclic voltammetry and galvanostatic spectroscopy at room temperature using 0.5 M  $\text{H}_2\text{SO}_4$  as the electrolyte in a three-electrode cell using an Autolab PGSTAT302 electrochemical test system (Eco Chemie, The Netherlands). Electrochemical impedance spectroscopy measurements were carried out over a frequency range from 10 kHz to 10 mHz in a 1 M  $\text{H}_2\text{SO}_4$  electrolyte. The applied voltage was 10 mV. The working electrode was fabricated by casting deionized (DI) water-impregnated graphene ink onto a 5 mm diameter vitreous glassy carbon electrode. To prepare the graphene ink, 20 mg of a graphene/PANI was ultrasonically dispersed into 5 mL of DI water. A 20  $\mu\text{L}$  portion of the graphene/PANI ink was coated on the electrode and dried at  $60^\circ\text{C}$ . Then, 5  $\mu\text{L}$  of Nafion solution containing 2-propanol (5 wt %, Dupont) was deposited on the electrode.

A capacitor was fabricated with  $\text{NH}_2\text{-RG-O/PANI}$  and N-RG-O electrodes, which were separated by filter paper in 1 M  $\text{H}_2\text{SO}_4$  electrolyte. The working electrode was prepared by mixing  $\text{NH}_2\text{-RG-O/PANI}$  or N-RG-O (80 wt %) with PVDF binder (10 wt %) and carbon black (10 wt %), and then the thin film prepared by a roll to roll process. The  $\text{NH}_2\text{-RG-O/PANI}$  thin film was then cut into disks with a diameter of 1 cm. The weights of  $\text{NH}_2\text{-RG-O/PANI}$  and N-RG-O were 2.0 and 3.0 mg.

**Conflict of Interest:** The authors declare no competing financial interest.

**Supporting Information Available:** FT-IR and C1s XPS spectra of G-O, RG-O,  $\text{NH}_2\text{-G-O}$ , and N-RG-O. This material is available free of charge *via* the Internet at <http://pubs.acs.org>.

## REFERENCES AND NOTES

- Frackowiak, E. Carbon Materials for Supercapacitor Application. *Phys. Chem. Chem. Phys.* **2007**, *9*, 1774–1785.
- Inagaki, M.; Konno, H.; Tanaike, O. Carbon Materials for Electrochemical Capacitors. *J. Power Sources* **2010**, *195*, 7880–7903.
- Wu, Z. S.; Wang, D. W.; Ren, W.; Zhao, J.; Zhou, G.; Li, F.; Cheng, H. M. Anchoring Hydrous RuO<sub>2</sub> on Graphene Sheets for High-Performance Electrochemical Capacitors. *Adv. Funct. Mater.* **2010**, *20*, 3595–3602.
- Hu, C. C.; Tsou, T. W. Ideal Capacitive Behavior of Hydrous Manganese Oxide Prepared by Anodic Deposition. *Electrochem. Commun.* **2002**, *4*, 105–109.
- Wang, D. W.; Li, F.; Zhao, J. P.; Ren, W. C.; Chen, Z. G.; Tan, J.; Wu, Z. S.; Gentle, I.; Lu, G. Q.; Cheng, H. M. Fabrication of Graphene/Polyaniline Composite Paper via *in Situ* Anodic Electropolymerization for High-Performance Flexible Electrode. *ACS Nano* **2009**, *3*, 1745–1752.
- Zhang, L. L.; Zhao, S. Y.; Tian, X. N.; Zhao, X. S. Layered Graphene Oxide Nanostructures with Sandwiched Conducting Polymers as Supercapacitor Electrodes. *Langmuir* **2010**, *26*, 17624–17628.
- Snook, G. A.; Kao, P.; Best, A. S. Conducting-Polymer-Based Supercapacitor Devices and Electrodes. *J. Power Sources* **2011**, *196*, 1–12.
- Tu, L. L.; Jia, C. Y. Conducting Polymers as Electrode Materials for Supercapacitors. *Prog. Chem.* **2010**, *22*, 1610–1618.
- Xu, J. J.; Wang, K.; Zu, S. Z.; Han, B. H.; Wei, Z. X. Hierarchical Nanocomposites of Polyaniline Nanowire Arrays on Graphene Oxide Sheets with Synergistic Effect for Energy Storage. *ACS Nano* **2010**, *4*, 5019–5026.
- Wang, H. L.; Hao, Q. L.; Yang, X. J.; Lu, L. D.; Wang, X. A Nanostructured Graphene/polyaniline Hybrid Material for Supercapacitors. *Nanoscale* **2010**, *2*, 2164–2170.
- Meng, C. Z.; Liu, C. H.; Fan, S. S. Flexible Carbon Nanotube/Polyaniline Paper-like Films and Their Enhanced Electrochemical Properties. *Electrochem. Commun.* **2009**, *11*, 186–189.
- Girija, T. C.; Sangaranarayanan, M. V. Analysis of Polyaniline-Based Nickel Electrodes for Electrochemical Supercapacitors. *J. Power Sources* **2006**, *156*, 705–711.
- Hu, Z. A.; Xie, Y. L.; Wang, Y. X.; Mo, L. P.; Yang, Y. Y.; Zhang, Z. Y. Polyaniline/SnO<sub>2</sub> Nanocomposite for Supercapacitor Applications. *Mater. Chem. Phys.* **2009**, *114*, 990–995.
- Stankovich, S.; Dikin, D. A.; Dommett, G. H. B.; Kohlhaas, K. M.; Zimney, E. J.; Stach, E. A.; Piner, R. D.; Nguyen, S. T.; Ruoff, R. S. Graphene-Based Composite Materials. *Nature* **2006**, *442*, 282–286.
- Gomez, H.; Ram, M. K.; Alvi, F.; Villalba, P.; Stefanakos, E.; Kumar, A. Graphene-Conducting Polymer Nanocomposite as Novel Electrode for Supercapacitors. *J. Power Sources* **2011**, *196*, 4102–4108.
- Yang, N. L.; Zhai, J.; Wan, M. X.; Wang, D.; Jiang, L. Layered Nanostructures of Polyaniline with Graphene Oxide as the Dopant and Template. *Synth. Met.* **2010**, *160*, 1617–1622.
- Ryu, K. S.; Kim, K. M.; Park, N. G.; Park, Y. J.; Chang, S. H. Symmetric Redox Supercapacitor with Conducting Polyaniline Electrodes. *J. Power Sources* **2002**, *103*, 305–309.
- Hummers, W. S.; Offeman, R. E. Preparation of Graphite Oxide. *J. Am. Chem. Soc.* **1958**, *80*, 1339–1339.
- Wang, H. L.; Hao, Q. L.; Yang, X. J.; Lu, L. D.; Wang, X. Graphene Oxide Doped Polyaniline for Supercapacitors. *Electrochem. Commun.* **2009**, *11*, 1158–1161.
- Shafeeyan, M. S.; Daud, W.; Houshmand, A.; Shamiri, A. A Review on Surface Modification of Activated Carbon for Carbon Dioxide Adsorption. *J. Anal. Appl. Pyrolysis* **2010**, *89*, 143–151.
- Lai, L. F.; Chen, L. W.; Zhan, D.; Sun, L.; Liu, J. P.; Lim, S. H.; Poh, C. K.; Shen, Z. X.; Lin, J. Y. One-Step Synthesis of NH<sub>2</sub>-Graphene from *in Situ* Graphene-Oxide Reduction and Its Improved Electrochemical Properties. *Carbon* **2011**, *49*, 3250–3257.
- Shin, H. J.; Kim, K. K.; Benayad, A.; Yoon, S. M.; Park, H. K.; Jung, I. S.; Jin, M. H.; Jeong, H. K.; Kim, J. M.; Choi, J. Y.; *et al.* Efficient Reduction of Graphite Oxide by Sodium Borohydride and Its Effect on Electrical Conductance. *Adv. Funct. Mater.* **2009**, *19*, 1987–1992.
- Loh, K. P.; Bao, Q. L.; Eda, G.; Chhowalla, M. Graphene Oxide as a Chemically Tunable Platform for Optical Applications. *Nat. Chem.* **2010**, *2*, 1015–1024.
- Pacile, D.; Papagno, M.; Rodriguez, A. F.; Grioni, M.; Papagno, L. Near-Edge X-ray Absorption Fine-Structure Investigation of Graphene. *Phys. Rev. Lett.* **2008**, *101*, 668061–4.
- Jeong, H. K.; Colakerol, L.; Jin, M. H.; Glans, P. A.; Smith, K. E.; Lee, Y. H. Unoccupied Electronic States in Graphite Oxides. *Chem. Phys. Lett.* **2008**, *460*, 499–502.
- Hua, W. J.; Gao, B.; Li, S. H.; Agren, H.; Luo, Y. X-ray Absorption Spectra of Graphene from First-Principles Simulations. *Phys. Rev. B* **2010**, *82*, 155433–40.
- Abbas, G.; Papakonstantinou, P.; Iyer, G. R. S.; Kirkman, I. W.; Chen, L. C. Substitutional Nitrogen Incorporation through Rf Glow Discharge Treatment and Subsequent Oxygen Uptake on Vertically Aligned Carbon Nanotubes. *Phys. Rev. B* **2007**, *75*, 1954291–9.
- Roy, S. S.; McCann, R.; Papakonstantinou, P.; Maguire, P.; McLaughlin, J. A. The Structure of Amorphous Carbon Nitride Films Using a Combined Study of NEXAFS, XPS and Raman Spectroscopies. *Thin Solid Films* **2005**, *482*, 145–150.
- Zhang, L. S.; Liang, X. Q.; Song, W. G.; Wu, Z. Y. Identification of the Nitrogen Species on N-Doped Graphene Layers and Pt/NG Composite Catalyst for Direct Methanol Fuel Cell. *Phys. Chem. Chem. Phys.* **2010**, *12*, 12055–12059.
- Jansen, R. J. J.; Vanbekkum, H. XPS of Nitrogen-Containing Functional Groups on Activated Carbon. *Carbon* **1995**, *33*, 1021–1027.
- Wu, Q.; Xu, Y. X.; Yao, Z. Y.; Liu, A. R.; Shi, G. Q. Supercapacitors Based on Flexible Graphene/Polyaniline Nanofiber Composite Films. *ACS Nano* **2010**, *4*, 1963–1970.
- Yan, J.; Wei, T.; Shao, B.; Fan, Z. J.; Qian, W. Z.; Zhang, M. L.; Wei, F. Preparation of a Graphene Nanosheet/Polyaniline Composite with High Specific Capacitance. *Carbon* **2010**, *48*, 487–493.
- Zhang, K.; Zhang, L. L.; Zhao, X. S.; Wu, J. S. Graphene/Polyaniline Nanoribber Composites as Supercapacitor Electrodes. *Chem. Mater.* **2010**, *22*, 1392–1401.
- Kim, J. H.; Sharma, A. K.; Lee, Y. S. Synthesis of Polypyrrole and Carbon Nano-fiber Composite for the Electrode of Electrochemical Capacitors. *Mater. Lett.* **2006**, *60*, 1697–1701.
- Frackowiak, E.; Beguin, F. Electrochemical Storage of Energy in Carbon Nanotubes and Nanostructured Carbons. *Carbon* **2002**, *40*, 1775–1787.
- Aboutaleb, S. H.; Chidembo, A. T.; Salari, M.; Konstantinov, K.; Wexler, D.; Liu, H. K.; Dou, S. X. Comparison of GO, GO/MWCNTs Composite and MWCNTs as Potential Electrode Materials for Supercapacitors. *Energy Environ. Sci.* **2011**, *4*, 1855–1865.
- Fang, B.; Wei, Y. Z.; Suzuki, K.; Kumagai, A. Surface Modification of Carbonaceous Materials for EDLCs Application. *Electrochim. Acta* **2005**, *50*, 3616–3621.
- Lozano-Castello, D.; Cazorla-Amoros, D.; Linares-Solano, A.; Shiraishi, S.; Kurihara, H.; Oya, A. Influence of Pore Structure and Surface Chemistry on Electric Double Layer Capacitance in Non-aqueous Electrolyte. *Carbon* **2003**, *41*, 1765–1775.
- Bleda-Martinez, M. J.; Macia-Agullo, J. A.; Lozano-Castello, D.; Morallon, E.; Cazorla-Amoros, D.; Linares-Solano, A. Role of Surface Chemistry on Electric Double Layer Capacitance of Carbon Materials. *Carbon* **2005**, *43*, 2677–2684.
- Shen, J. M.; Liu, A. D.; T. Y.; Foo, G. S.; Yeo, C. B.; Chan-Park, M. B.; Jiang, R. R.; Chen, Y. How Carboxylic Groups Improve the Performance of Single-Walled Carbon Nanotube Electrochemical Capacitors. *Energy Environ. Sci.* **2011**, *10*, 4220–4229.
- Masarapu, C.; Zeng, H. F.; Hung, K. H.; Wei, B. Q. Effect of Temperature on the Capacitance of Carbon Nanotube Supercapacitors. *ACS Nano* **2009**, *3*, 2199–2206.

42. Abidian, M. R.; Martin, D. C. Experimental and Theoretical Characterization of Implantable Neural Microelectrodes Modified with Conducting Polymer Nanotubes. *Biomaterials* **2008**, *29*, 1273–1283.
43. Li, X.; Rong, J. P.; Wei, B. Q. Electrochemical Behavior of Single-Walled Carbon Nanotube Supercapacitors under Compressive Stress. *ACS Nano* **2010**, *4*, 6039–6049.
44. Stoller, M. D.; Ruoff, R. S. Best Practice Methods for Determining an Electrode Material's Performance for Ultracapacitors. *Energy Environ. Sci.* **2010**, *3*, 1294–1301.
45. Khomenko, V.; Frackowiak, E.; Beguin, F. Determination of the Specific Capacitance of Conducting Polymer/Nanotubes Composite Electrodes Using Different Cell Configurations. *Electrochim. Acta* **2005**, *50*, 2499–2506.